# Weak-force sensing in an optomechanical system with squeezed light and feedback control

Doudou Wang [1], Suqin Hu [1], Qiang Zhang,[1,2] and Yongmin Li [1,2,*]

[1]*State Key Laboratory of Quantum Optics Technologies and Devices, Institute of Opto-Electronics, Shanxi University, Taiyuan, Shanxi 030006, China*

[2]*Collaborative Innovation Center of Extreme Optics, Shanxi University, Taiyuan, Shanxi 030006, China*

(Received 9 December 2025; accepted 27 March 2026; published 17 April 2026)

We propose a high-precision weak-force sensing scheme with squeezed light and feedback control in an unresolved-sideband cavity optomechanical system. This scheme employs synergistic integration of the injection of squeezed light and measurement-based feedback control. We analyze the influence mechanism of various system parameters and examine how squeezed light and closed-loop control jointly improve the measurement sensitivity. The proposed weak-force sensing scheme could improve the signal-to-noise ratio of the weak-force measurement and reduce the added noises. It is compatible with state-of-the-art cavity optomechanical techniques and may find applications in quantum metrology, gravitational wave detection, and fundamental physics tests.

DOI: 10.1103/9tkg-6xxc

## I. INTRODUCTION

In precision measurement [1,2], the detection of weak forces is of paramount importance. This capability is fundamental to several critical research directions, such as gravitational wave detection [3,4], studies of the Casimir force [5], characterization of intermolecular forces [6], force microscopy [7], and the exploration of new physics. At the attonewton ($10^{-18}$ N) scale [8,9], the pursuit of high-sensitivity broadband force detection is increasingly constrained by the standard quantum limit (SQL).

In quantum-enhanced sensing, squeezed light has proven to be a useful resource for improving sensitivity [10–13]. By injecting squeezed light into the output dark port, quantum correlations between light and the kilogram-mass mirrors of LIGO were observed, which enables the sub-SQL displacement measurement to be achieved [14]. Subsequently, it was shown that intracavity squeezing could allow the detection of weak forces with enhanced precision [15–17]. The synergistic integration of intracavity squeezing (ICS) and extracavity squeezing (ECS) can exponentially increase the signal-to-noise ratio (SNR) for dispersive qubit readout [18] and temperature metrology [19].

Another powerful approach to sensitivity enhancement is measurement-based feedback control [20]. Bemani *et al*. [21] proposed a feedback-controlled in-loop light scheme for an optomechanical force sensor, enabling simultaneous signal amplification (via enhanced mechanical response) and noise suppression below the SQL. Their work focuses mainly on the force sensor in the red-detuned resolved-sideband regime. By using the Floquet approach, it briefly investigates the system dynamics beyond the rotating-wave approximation and discusses the case of weak-force measurement in the unresolved-sideband regime.

Note that the measurement-based feedback control is analogous to ICS; more precisely, both of them can generate self-parametric interaction of intracavity optical fields. Due to the fact that the ICS requires additional pump light, a nonlinear medium in the cavity, and stringent phase-matching conditions, its realization is a challenge. In comparison, feedback control only relies on the detection and modulation of the probe field outside the cavity; therefore, it is technically more feasible. It is reasonable to expect that combining ECS with feedback control could significantly enhance the measurement sensitivity.

In this paper we propose a high-precision weak-force sensor using an unresolved-sideband cavity optomechanical system with squeezed light and feedback control. Feedback control can effectively enhance the mechanical response of the optomechanical system to external force while inducing low added noise of measurement. For a nonzero optical detuning, the injection of squeezed light can suppress the detection noises via inducing the quantum correlations between the optical mode and mechanical mode. Both methods jointly boost the measurement sensitivity.

This paper is organized as follows. In Sec. II we present the system Hamiltonians and derive the force sensitivity. In Sec. III we analyze the effects of the relevant system parameters on the force measurement at both the resonance and detuning regions, after accounting for measurement-induced frequency shifts. In Sec. IV we explicitly discuss the experimental feasibility of the proposed weak-force sensor. In Sec. V we summarize and offer prospects for future work.

## II. METHODS

Our scheme for the weak-force sensor is depicted in Fig. 1. An optomechanical system is probed with squeezed light, which carries the weak-force signal $F$ to the balanced homodyne detector for readout. The resulting photocurrent $i_{\rm fb}(t)$ is fed back to the input probe field using an amplitude modulator that modulates the amplitude of the input light. Subsequently, the standard linear-response theory can be employed to estimate the external force.

*Contact author: yongmin@sxu.edu.cn

 

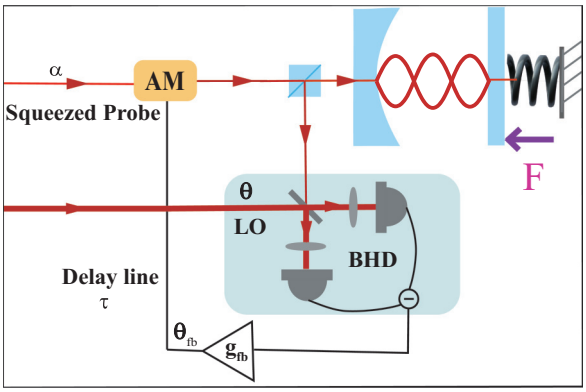


FIG. 1. Schematic of the proposed optomechanical force sensor. A bright squeezed light with variable squeezed phase $\alpha$ is injected into the optomechanical system, where a mechanical oscillator subjected to a force $F(t)$ serves as one of the end mirrors in a high-finesse optical cavity. The photocurrent from the balanced homodyne detector (BHD), which measures the $\theta$-phase quadrature of the reflected light, is used as a feedback signal. This signal, with a gain of $g_{\rm fb}$ and a variable delay $\tau$, drives an amplitude modulator (AM) to control the input light's amplitude. Here LO denotes local oscillator.

### A. Heisenberg-Langevin equations and system dynamics

We consider a single mechanical mode coupled to an optical mode via radiation pressure. The time-dependent Hamiltonian describing this system is given by [22,23]

$$\hat{H} = \hbar\omega_{\rm c}\hat{c}^\dagger\hat{c} + \frac{\hbar\omega_m}{2}(\hat{Q}^2+\hat{P}^2) + \sqrt{2}\hbar g_{\rm s}\hat{c}^\dagger\hat{c}\hat{Q} + \sqrt{2}x_{\rm ZPF}\hat{F}(t)\hat{Q} + {\rm i}\hbar(\sqrt{\kappa_{\rm s1}}\epsilon_{\rm in}\hat{c}^\dagger e^{-{\rm i}\omega_{\rm l}t} + {\rm c.c.}). \quad (1)$$

The first and second terms describe the free energy of the cavity mode and the mechanical resonator, respectively, where $\hat{c}$ ($\hat{c}^\dagger$) is the annihilation (creation) operator of the cavity mode, $\omega_{\rm c}$ is the cavity resonance frequency, $\hat{Q} = (\hat{b}+\hat{b}^\dagger)/\sqrt{2}$, $\hat{P} = {\rm i}(\hat{b}^\dagger-\hat{b})/\sqrt{2}$, and $\hat{b}$ ($\hat{b}^\dagger$) is the annihilation (creation) operator of the mechanical mode with the characteristic frequency $\omega_m$. The third term describes the interaction between the cavity mode and the mechanical mode, where $g_s$ is the single-photon interaction rate. The fourth term in the Hamiltonian describes the coupling of the mechanical mode to an input classical ideal impulsive force $\hat{F}(t)$ in the $x$ direction and $x_{\rm ZPF} = \sqrt{\hbar/2m\omega_m}$ is the zero-point-position uncertainty of the resonator with effective mass $m$. The last term denotes the input probe field with frequency $\omega_{\rm l}$, $\kappa_{\rm s1}$ represents the cavity decay rate associated with the left mirror, $\epsilon_{\rm in}$ is the driving strength of the probe light, and c.c. stands for complex conjugate.

Considering the fluctuation and dissipation processes affecting the optical and mechanical modes, the general Markov Langevin equation for the mechanical mode and the rotating-wave Langevin equation for the optical mode are written as [24]

$$\dot{\hat{c}} = (-{\rm i}\Delta_{\rm s} - \kappa/2)\hat{c} - \sqrt{2}{\rm i}g_{\rm s}\hat{c}\hat{Q} + \sqrt{\kappa_{\rm s1}}(\epsilon_{\rm in}+\hat{c}_{\rm in}) + \sqrt{\kappa_{\rm s2}}\hat{c}_{\rm in2}, \quad (2a)$$

$$\dot{\hat{Q}} = \omega_m\hat{P}, \quad (2b)$$

$$\dot{\hat{P}} = -\omega_m\hat{Q} - \sqrt{2}g_{\rm s}\hat{c}^\dagger\hat{c} - \frac{1}{\sqrt{m\omega_m\hbar}}\hat{F} - \Gamma_m\hat{P} + \sqrt{2\Gamma_m}\hat{P}_{\rm in}, \quad (2c)$$

where $\Delta_{\rm s} = \omega_{\rm c} - \omega_{\rm l}$ is the detuning of the cavity resonance frequency $\omega_{\rm c}$ relative to the probe field frequency $\omega_{\rm l}$; $\hat{Q}$ and $\hat{P}$ are the dimensionless position and momentum quadrature's of the mechanical oscillator, respectively; $\kappa_{\rm s1}$ and $\kappa_{\rm s2}$ are the decay rates of the left and right mirrors of the optical cavity, respectively; $\kappa = \kappa_{\rm s1}+\kappa_{\rm s2}$; and $\Gamma_m = \omega_m/Q$ is the decay rate of the mechanical mode, with $Q$ the mechanical quality factor. Here the mechanical noise $\hat{P}_{in} = {\rm i}(\hat{b}_{\rm in}^\dagger - \hat{b}_{\rm in})/\sqrt{2}$ affecting the nanomechanical oscillators satisfies the Markovian correlation functions

$$\langle\hat{P}_{\rm in}(t)\hat{P}_{\rm in}(t')\rangle = (\bar{n}_{\rm th}+\tfrac{1}{2})\delta(t-t'), \quad (3a)$$

$$\bar{n}_{\rm th} = 1/[\exp(\hbar\omega_m/k_{\rm B}T)-1], \quad (3b)$$

where $\bar{n}_{\rm th}$ is the mean number of the thermal excitations of the mechanical bath at temperature $T$. The probe field is squeezed and satisfies [12,19,25]

$$\langle\hat{c}_{\rm in}(t)\hat{c}_{\rm in}^\dagger(t')\rangle = [1+\zeta\sinh^2(r)]\delta(t-t'), \quad (4a)$$

$$\langle\hat{c}_{\rm in}^\dagger(t)\hat{c}_{\rm in}(t')\rangle = \zeta\sinh^2(r)\delta(t-t'), \quad (4b)$$

$$\langle\hat{c}_{\rm in}^\dagger(t)\hat{c}_{\rm in}^\dagger(t')\rangle = \tfrac{1}{2}e^{-2{\rm i}\alpha}\zeta\sinh(2r)\delta(t-t'), \quad (4c)$$

$$\langle\hat{c}_{\rm in}(t)\hat{c}_{\rm in}(t')\rangle = \tfrac{1}{2}e^{2{\rm i}\alpha}\zeta\sinh(2r)\delta(t-t'), \quad (4d)$$

where $\zeta$ denotes the output-coupling efficiency of the optical parametric oscillator, which is employed to prepare the squeezing light, and $\alpha = 0$ ($\pi/2$) denotes phase (amplitude) quadrature squeezing.

We consider weak optomechanical coupling and a strongly driven optical cavity field. This allows us to linearize the quantum dynamics of fluctuations around the mean amplitudes [24,26] $\hat{c} = \epsilon + \delta\hat{c}$ and $\hat{b} = \beta + \delta\hat{b}$. The effective coupling strength between the optical field and the mechanical resonator after the linearization procedure is defined as $G = g_{\rm s}\epsilon$. By omitting the $\delta$ symbols in the quantum fluctuations, the linearized optomechanical Langevin equations are given by

$$\dot{\hat{c}} = (-{\rm i}\Delta - \kappa/2)\hat{c} - \sqrt{2}{\rm i}G\hat{Q} + \sqrt{\kappa_{\rm s1}}\hat{c}_{\rm in} + \sqrt{\kappa_{\rm s2}}\hat{c}_{\rm in2}, \quad (5a)$$

$$\dot{\hat{b}} = (-{\rm i}\omega_m - \Gamma_m/2)\hat{b} + \frac{\Gamma_m}{2}\hat{b}^\dagger - {\rm i}G(\hat{c}+\hat{c}^\dagger) + \sqrt{\Gamma_m}\hat{b}_{\rm in,f}, \quad (5b)$$

where $\Delta = \Delta_{\rm s} + g_{\rm s}(\beta+\beta^*)$ is the effective detuning of the probe laser [24]. The input mechanical operator $\hat{b}_{\rm in,f}(t)$ combines the external force to be detected $F(t)$ and a noise operator, representing the total stochastic drive on the system [22]

$$\hat{b}_{\rm in,f}(t) = -{\rm i}\frac{1}{\sqrt{2m\omega_m\hbar\Gamma_m}}\hat{F}(t) + \frac{1}{\sqrt{2}}\hat{b}_{\rm in}(t) - \frac{1}{\sqrt{2}}\hat{b}_{\rm in}^\dagger(t). \quad (6)$$

Next we introduce the feedback control in the system dynamics. The reflected field $\hat{c}_{\rm out}$ is defined via the input-output

relation [26]

$$\hat{c}_{\rm out}(t) = -\sqrt{\kappa_{\rm s1}}\hat{c}(t) + \hat{c}_{\rm in}(t). \tag{7}$$

We implement the phase-sensitive detection of the quadrature at phase $\theta$,

$$\hat{X}^{\theta}_{\rm out}(t) = \frac{e^{-{\rm i}\theta}\hat{c}_{\rm out}(t) + e^{{\rm i}\theta}\hat{c}^{\dagger}_{\rm out}(t)}{\sqrt{2}}. \tag{8}$$

The photocurrent measured by the homodyne detector is given by

$$i_{\rm fb}(t) = \sqrt{\eta}\hat{X}^{\theta}_{\rm out}(t) + \sqrt{1-\eta}\hat{X}^{\theta}_{\rm v}(t), \tag{9}$$

where the vacuum noise operator $\hat{X}_{\rm v}(t)$ satisfies the autocorrelation relation $\langle \hat{X}_{\rm v}(t)\hat{X}_{\rm v}(t')\rangle = \frac{1}{2}\delta(t-t')$. The effective detection efficiency $\eta$ consists of three parts: detector quantum efficiency $\eta_{\rm q}$, optical propagation efficiency $\eta_{\rm o}$, and equivalent efficiency arising from the detector electronic noises $\eta = \eta_{\rm q}\eta_{\rm o}/(1 + S_{\rm e}/S_{\rm sn})$. Here $S_{\rm e}/S_{\rm sn}$ denotes the electronic-to-shot-noise ratio [23].

By assuming the filter function $g_{\rm fb}$ is constant in the relevant frequency band [21] and a finite feedback delay time $\tau$, the input probe field with the feedback loop is written as

$$\hat{c}_{\rm in}(t) = \hat{c}_{\rm in,0}(t) + g_{\rm fb} i_{\rm fb}(t-\tau). \tag{10}$$

Here $\hat{c}_{\rm in,0}(t)$ is the original input probe field and $g_{\rm fb}$ is the feedback gain. Neglecting the dispersion effects of the electronic feedback loop, the photocurrent is given by

$$\begin{aligned} i_{\rm fb}(t-\tau) = &-e^{-{\rm i}\theta}\sqrt{\frac{\eta\kappa_{\rm s1}}{2}}\hat{c}(t-\tau) + e^{-{\rm i}\theta}\sqrt{\frac{\eta}{2}}\hat{c}_{\rm in}(t-\tau) \\ &- e^{{\rm i}\theta}\sqrt{\frac{\eta\kappa_{\rm s1}}{2}}\hat{c}^{\dagger}(t-\tau) + e^{{\rm i}\theta}\sqrt{\frac{\eta}{2}}\hat{c}^{\dagger}_{\rm in}(t-\tau) \\ &+ g_{\rm fb}\sqrt{1-\eta}\hat{X}^{\theta}_{\rm v}(t-\tau). \end{aligned} \tag{11}$$

By taking the Fourier transform of all the terms via $o[\omega] = \int_{-\infty}^{\infty} dt\, e^{{\rm i}\omega t} o(t)$, we write the Eq. (11) in the frequency domain

$$\begin{aligned} i_{\rm fb}[\omega]e^{{\rm i}\omega\tau} = &-e^{-{\rm i}(\theta-\omega\tau)}\sqrt{\frac{\eta\kappa_{\rm s1}}{2}}\hat{c}[\omega] + e^{-{\rm i}(\theta-\omega\tau)}\sqrt{\frac{\eta}{2}}\hat{c}_{\rm in}[\omega] \\ &- e^{{\rm i}(\theta+\omega\tau)}\sqrt{\frac{\eta\kappa_{\rm s1}}{2}}\hat{c}^{\dagger}[\omega] + e^{{\rm i}(\theta+\omega\tau)}\sqrt{\frac{\eta}{2}}\hat{c}^{\dagger}_{\rm in}[\omega] \\ &+ g_{\rm fb}e^{{\rm i}\omega\tau}\sqrt{1-\eta}\hat{X}^{\theta}_{\rm v}[\omega]. \end{aligned} \tag{12}$$

The equation of motion of the cavity field is obtained by combining Eqs. (5a) and (10)–(12),

$$\begin{aligned} -{\rm i}\omega\hat{c}[\omega] = &(-{\rm i}\Delta - \kappa_{\rm fb}/2)\hat{c}[\omega] + \Lambda\hat{c}^{\dagger}[\omega] \\ &- {\rm i}G(\hat{b}[\omega] + \hat{b}^{\dagger}[\omega]) + \sqrt{\kappa_{\rm fb}}\hat{c}_{\rm in,fb}[\omega], \end{aligned} \tag{13}$$

where

$$\begin{aligned} \hat{c}_{\rm in,fb}[\omega] = \frac{1}{\sqrt{\kappa_{\rm fb}}}\Bigg[&\left(\sqrt{\kappa_{\rm s1}} + \frac{\mu}{\sqrt{\kappa_{\rm s1}}}e^{{\rm i}(\theta_{\rm fb}-\theta)}\right)\hat{c}_{\rm in}[\omega] \\ &+ \frac{\mu}{\sqrt{\kappa_{\rm s1}}}e^{{\rm i}(\theta_{\rm fb}+\theta)}\hat{c}^{\dagger}_{\rm in}[\omega] + g_{\rm fb}e^{{\rm i}(\theta_{\rm fb}+\theta)} \\ &\times\sqrt{\frac{\kappa_{\rm s1}(1-\eta)}{2}}\hat{c}^{\dagger}_{\rm v}[\omega] + g_{\rm fb}e^{{\rm i}(\theta_{\rm fb}-\theta)}\sqrt{\frac{\kappa_{\rm s1}(1-\eta)}{2}} \\ &\times\hat{c}_{\rm v}[\omega] + \sqrt{\kappa_{\rm s2}}\hat{c}_{\rm in2}[\omega]\Bigg], \end{aligned} \tag{14}$$

with $\theta_{\rm fb} = \omega\tau$. The feedback-modified cavity decay rate is $\kappa_{\rm fb} = \kappa + 2\mu e^{{\rm i}(\theta_{\rm fb}-\theta)}$, where $\mu = \kappa_{\rm s1}g_{\rm fb}\sqrt{\eta/2}$. In addition, $\Lambda = -\mu e^{{\rm i}(\theta_{\rm fb}+\theta)}$ represents the parametric coupling strength between the annihilation operator $\hat{c}$ and creation operator $\hat{c}^{\dagger}$ of the feedback-induced optical field mode, analogous to the self-parametric interaction of intracavity optical fields [16,27,28]. In the intracavity squeezing model, the equivalent parameter $\Lambda$ is defined as $2{\rm i}\xi$, with $\xi$ a complex parameter quantifying the intracavity squeezing coupling strength. Under specific conditions, quantum feedback control offers a viable alternative capable of supplanting the intracavity squeezing scheme. This coupling strength governs the nonlinear behavior of the optical field and also indicates that the system meets the minimum requirements for feedback-enhanced sensing [29]. The equations of motion can be summarized in the matrix form

$$-{\rm i}\omega\hat{u}[\omega] = A\hat{u}[\omega] + H\hat{n}_{\rm in,fb}[\omega], \tag{15}$$

where

$$\hat{u}[\omega] = [\hat{c}[\omega], \hat{c}^{\dagger}[\omega], \hat{b}[\omega], \hat{b}^{\dagger}[\omega]]^{T}, \tag{16a}$$

$$H = {\rm diag}[\sqrt{\kappa_{\rm fb}}, \sqrt{\kappa^{*}_{\rm fb}}, \sqrt{\Gamma_m}, \sqrt{\Gamma_m}], \tag{16b}$$

$$\hat{n}_{\rm in,fb}[\omega] = [\hat{c}_{\rm in,fb}[\omega], \hat{c}^{\dagger}_{\rm in,fb}[\omega], \hat{b}_{\rm in,f}[\omega], \hat{b}^{\dagger}_{\rm in,f}[\omega]]^{T}. \tag{16c}$$

The drift matrix $A$ is defined as

$$A = \begin{Bmatrix} -{\rm i}\Delta - \kappa_{\rm fb}/2 & \Lambda & -{\rm i}G & -{\rm i}G \\ \Lambda^{*} & {\rm i}\Delta - \kappa^{*}_{\rm fb}/2 & {\rm i}G & {\rm i}G \\ -{\rm i}G & -{\rm i}G & -{\rm i}\omega_m - \Gamma_m/2 & \Gamma_m/2 \\ {\rm i}G & {\rm i}G & \Gamma_m/2 & {\rm i}\omega_m - \Gamma_m/2 \end{Bmatrix}. \tag{17}$$

Stability requires that all eigenvalues of the matrix $A$ reside in the closed left half plane. This condition, derived using the Routh-Hurwitz criterion, is detailed in Appendix B. The solution of Eq. (15) in the frequency domain is given by

$$\hat{u}[\omega] = (-{\rm i}\omega I_{4\times4} - A)^{-1}H\hat{n}_{\rm in,f}[\omega]. \tag{18}$$

By substituting $\hat{u}(\omega)$ into the input-output relation $\hat{n}_{\rm out}[\omega] = -M\hat{u}[\omega] + \hat{n}_{\rm in}[\omega]$, we have

$$\begin{aligned} \hat{n}_{\rm out}[\omega] &= M({\rm i}\omega I_{4\times4} + A)^{-1}H\hat{n}_{\rm in,fb}[\omega] + \hat{n}_{\rm in}[\omega] \\ &= S[\omega]\hat{n}_{\rm in,fb}[\omega] + \hat{n}_{\rm in}[\omega], \end{aligned} \tag{19}$$

$$\hat{n}_{\rm in}[\omega] = [\hat{c}_{\rm in}[\omega], \hat{c}^{\dagger}_{\rm in}[\omega], \hat{b}_{\rm in,f}[\omega], \hat{b}^{\dagger}_{\rm in,f}[\omega]]^T, \quad (20a)$$

$$\hat{n}_{\rm out}[\omega] = [\hat{c}_{\rm out}[\omega], \hat{c}^{\dagger}_{\rm out}[\omega], \hat{b}_{\rm out}[\omega], \hat{b}^{\dagger}_{\rm out}[\omega]]^T, \quad (20b)$$

$$M = {\rm diag}(\sqrt{\kappa_{\rm s1}}, \sqrt{\kappa_{\rm s1}}, \sqrt{\Gamma_m}, \sqrt{\Gamma_m}). \quad (20c)$$

We also define the scattering matrix $S[\omega]$,

$$S[\omega] = M({\rm i}\omega I_{4\times4} + A)^{-1}H, \quad (21)$$

where $I_{4\times4}$ is the identity matrix. The scattering matrix elements are given in Appendix A.

### B. Force measurement

An external force displaces the mechanical resonator from its equilibrium position and alters the cavity field via optomechanical coupling. Consequently, the external force signal can be extracted by measuring the generalized in-loop quadrature of the optical output $\hat{X}^{\theta}_{\rm out}[\omega]$,

$$\begin{aligned}\hat{X}^{\theta}_{\rm out}[\omega] = \frac{1}{\sqrt{2}}(&\Psi[\omega]\hat{c}_{\rm in,fb}[\omega] + \Psi^*[\omega]\hat{c}^{\dagger}_{\rm in,fb}[\omega] \\ &+ \Phi[\omega]\hat{b}_{\rm in,f}[\omega] + \Phi^*[\omega]\hat{b}^{\dagger}_{\rm in,f}[\omega] \\ &+ e^{-{\rm i}\theta}\hat{c}_{\rm in}[\omega] + e^{{\rm i}\theta}\hat{c}^{\dagger}_{\rm in}[\omega]).\end{aligned} \quad (22)$$

Here the functions $\Psi[\omega]$ and $\Phi[\omega]$ are defined as [21]

$$\Psi[\omega] = e^{-{\rm i}\theta}S_{11} + e^{{\rm i}\theta}S_{21}, \quad (23)$$

$$\Psi^*[\omega] = e^{-{\rm i}\theta}S_{12} + e^{{\rm i}\theta}S_{22}, \quad (24)$$

$$\Phi[\omega] = e^{-{\rm i}\theta}S_{13} + e^{{\rm i}\theta}S_{23}, \quad (25)$$

$$\Phi^*[\omega] = e^{-{\rm i}\theta}S_{14} + e^{{\rm i}\theta}S_{24}. \quad (26)$$

The reflected optical quadrature naturally combines the external force $\hat{X}^{\theta}_{\hat{F}}$ and the quantum noise $\hat{X}^{\theta}_{\rm out}|_{\hat{F}=0}$. The contribution of the external force is

$$\begin{aligned}\hat{X}^{\theta}_{\hat{F}} &= \sqrt{\frac{\eta}{2}}\frac{\rm i}{\sqrt{2m\omega_m\hbar\Gamma_m}}(\Phi^*[\omega]\hat{F}[\omega] - \Phi[\omega]\hat{F}[\omega]) \\ &= \frac{{\rm i}\sqrt{\eta}}{\sqrt{2m\omega_m\hbar\Gamma_m}}\bar{F}[\omega],\end{aligned} \quad (27)$$

where the transduction force is defined as [29]

$$\bar{F}[\omega] = \frac{1}{\sqrt{2}}[\Phi^*[\omega]\hat{F}^{\dagger}[\omega] - \Phi[\omega]\hat{F}[\omega]] \quad (28)$$

and $\sqrt{\eta}$ is from the effective detection efficiency ($\hat{X}^{\theta}_{\rm det} = \sqrt{\eta}(\hat{X}^{\theta}_{\rm out}[\omega]) + \sqrt{1-\eta}\hat{X}_{\rm v}$).

To estimate the sensitivity to external force, we define the effective force operator [21,29]

$$\hat{F}_{\rm eff}[\omega] = \frac{\hat{X}^{\theta}_{\rm det}[\omega]}{\partial\hat{X}^{\theta}_{\rm det}[\omega]/\partial\bar{F}[\omega]} = N^{\theta}[\omega] + \bar{F}[\omega]. \quad (29)$$

Here the noise force operator is given by

$$N^{\theta}[\omega] = \frac{\sqrt{2m\omega_m\hbar\Gamma_m}}{{\rm i}\sqrt{\eta}}\hat{X}^{\theta}_{\rm det}|_{\hat{F}=0}. \quad (30)$$

After calculations with the correlation in the frequency domain (note that the different noises are uncorrelated), the symmetrized power spectral density of the noise force $N^{\theta}[\omega]$ is given by

$$\overline{S}^{\theta}_{NN}[\omega] = 2m\omega_m\hbar\Gamma_m R_m[\omega]\{(\bar{n}_{\rm th} + \tfrac{1}{2}) + n_{\rm add}[\omega]\}, \quad (31)$$

where $R_m[\omega]$ is the mechanical response defined by

$$R_m[\omega] = \tfrac{1}{2}|\Phi^*[\omega] - \Phi[\omega]|^2 \quad (32)$$

and $n_{\rm add}$ is the noise of the measurement process. It combines backaction noise, imprecision noise, and the quantum correlations between imprecision and backaction (see Appendix D for details).

In the case of an ideal impulsive force $\hat{F}[\omega] = {\rm const}$, the spectral value of the force estimator becomes

$$S_{\bar{F}\bar{F}} = |\hat{F}|^2 R_m[\omega]. \quad (33)$$

Here $R_m[\omega] > 1$ indicates signal amplification. To characterize the force sensitivity, the SNR in the case of stationary spectral measurements is derived by using Eqs. (31) and (33),

$$\begin{aligned}{\rm SNR}[\omega] &= \sqrt{\frac{S_{\bar{F}\bar{F}}[\omega]}{S^{\theta}_{NN}[\omega]}} \\ &= \frac{|\hat{F}|}{\left\{2m\omega_m\hbar\Gamma_m\left(\bar{n}_{\rm th} + \frac{1}{2} + n_{\rm add}[\omega]\right)\right\}^{1/2}}.\end{aligned} \quad (34)$$

The system's force sensitivity, which describes the minimum magnitude of the input signal that can be reliably detected, is quantified using the relation ${\rm SNR}[\omega] = 1$ and has the form

$$S[\omega] = \left\{2m\omega_m\hbar\Gamma_m\left(\bar{n}_{\rm th} + \frac{1}{2} + n_{\rm add}[\omega]\right)\right\}^{1/2}. \quad (35)$$

TABLE I. Values of the parameters used in the numerical simulations.

| Parameter | Symbol | Value |
|---|---|---|
| Effective mass | $m$ | $10^{-12}$ kg |
| Mechanical frequency | $\omega_m$ | $2\pi \times 343.13$ kHz |
| Resonator decay rate | $\Gamma_m$ | $2\pi \times 1.18$ Hz |
| Cavity decay rate | $\kappa$ | $16\ \omega_m$ |
| Effective detection efficiency | $\eta$ | 0.9 |
| Decay rate of the left mirror | $\kappa_{\rm s1}$ | $0.95\ \kappa$ |
| Initial phonon number | $n_{\rm th}$ | 0 |
| Squeezing injection loss | $\zeta$ | 0.99 |

## III. RESULTS

In this section we analyze the effects of the relevant system parameters on the force measurement in both the resonance and detuning regimes. The simulation parameters, which are derived from a typical experimental setup of a membrane-in-the-middle cavity optomechanical system [30], are provided in Table I. We simulate the mechanical response, the added noises, and the force sensitivity using Eqs. (32), (D1), and (35), respectively. The unresolved-sideband regime is considered hereafter due to its greater technical feasibility. All results presented in Figs. 2–4 assume a thermal occupation number of $n_{\rm th} = 0$, corresponding to a ground-state cooled mechanical oscillator.

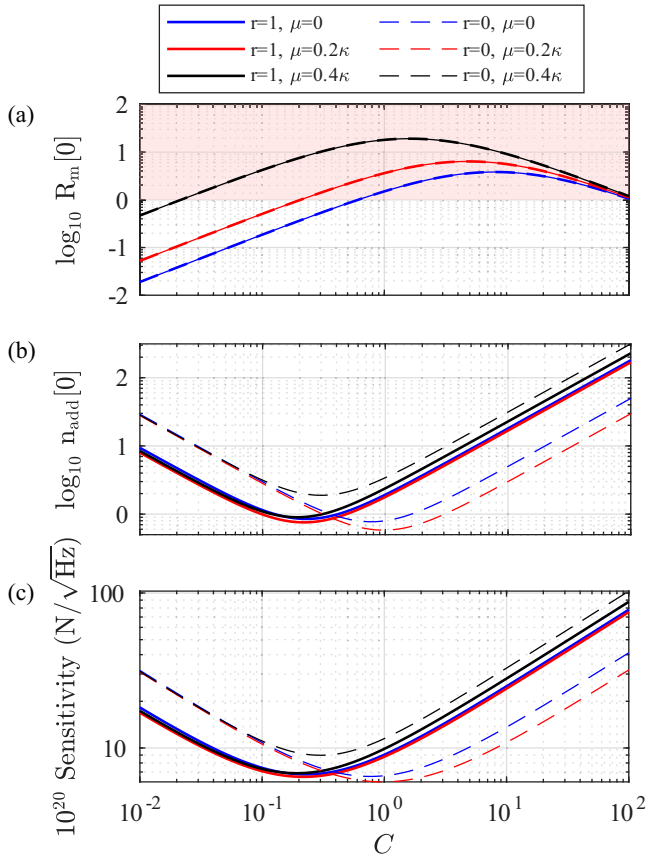


FIG. 2. (a) On-resonant mechanical response $R_m[0]$, (b) optically added noise of measurement $n_{\rm add}[0]$, and (c) force sensitivity at zero temperature as a function of the optomechanical cooperativity for different feedback gain. Solid lines represent squeezed light and dashed lines represent coherent light. The signal amplification ($R_m[0] > 1$) regions are shown by the red area. The parameters $\theta = 90^\circ$, $\alpha = 90^\circ$, $\theta_{\rm fb} = 270^\circ$, and $\Delta = \sqrt{\omega_m^2 + \kappa^2/4}$ are derived from Fig. 3. In addition, $r = 1$, The other parameters are given in Table I.

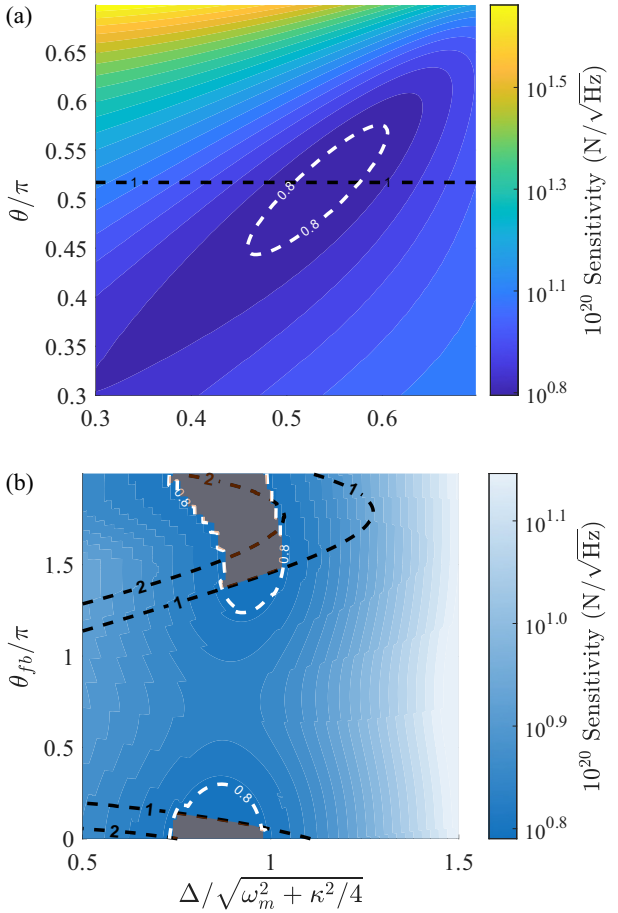


FIG. 3. (a) Force sensitivity as a function of the measurement angle $\theta$, squeezed angle $\alpha$, and fixed values of feedback phase $\theta_{\rm fb} = 270^\circ$ and laser detuning of $\Delta = \sqrt{\omega_m^2 + \kappa^2/4}$. The area below the black line ($R_m = 1$) and above the white line ($n_{\rm add}[0] < 0.8$) denotes the area that satisfies simultaneously noise reduction and signal amplification ($R_m[0] > 1$). (b) Force sensitivity at zero temperature as a function of the laser detuning $\Delta$, feedback delay angle $\theta_{\rm fb}$, and fixed values of the squeezed angle $\alpha = 90^\circ$ and the measurement angle $\theta = 90^\circ$. The transparent light gray shaded area denotes the region that satisfies simultaneously added noise suppression ($n_{\rm add}[0] < 0.8$) and signal amplification ($R_m[0] > 1$). Here $C = 0.25$, $\mu = 0.2\,\kappa$, and $r = 1$. The other parameters are given in Table I.

### A. On-resonance mechanical response and optically added noise

Figure 2(a) shows the on-resonant mechanical response $R_m[0]$ versus the optomechanical cooperativity $C$ for different feedback gain and squeezing levels. We see that a large gain is obtained at small cooperativities and a higher feedback gain. Squeezing has no effect on signal amplification.

Figure 2(b) shows that the feedback reduces the additional measurement noise at small optomechanical cooperativity and the appropriate choice of other parameters. The introduction of squeezing further suppresses the additional measurement noise. There exists an optimal optomechanical cooperativity to minimize measurement noises $n_{\rm add}[0]$, which depends on the balance between backaction noises and imprecision noises in the system [31]. In the absence of feedback force, both backaction noise and imprecision noise persist in the open-loop measurement. At the selected feedback delay phase, the mechanical oscillator response $R_m[0]$ and the backaction noise increase with the feedback gain, while the imprecision noise decreases with the feedback gain. Therefore, there exists an optimal gain that minimizes the measurement noise $n_{\rm add}[0]$ and maximizes the measurement sensitivity during the measurement. The optimal value of $\mu$ is determined by maximizing the force sensitivity. The feedback enhances the mechanical response to external signals by modifying the effective mechanical susceptibility. The measurement noise also depends on the feedback gain and phase. The signal-to-noise ratio (sensitivity) can be improved at appropriate feedback parameters.

Using the squeezing light associated with appropriate feedback, we get the highest force sensitivity at low optomechanical cooperativity, as shown in Fig. 2(c). We find that under current measurement conditions with $C = 0.1$, the squeezed light can achieve a 3.26-dB enhancement in force sensitivity at resonance compared to the coherent light. With the proper selection of feedback gain, the measurement sensitivity can be further increased by 0.43 dB.

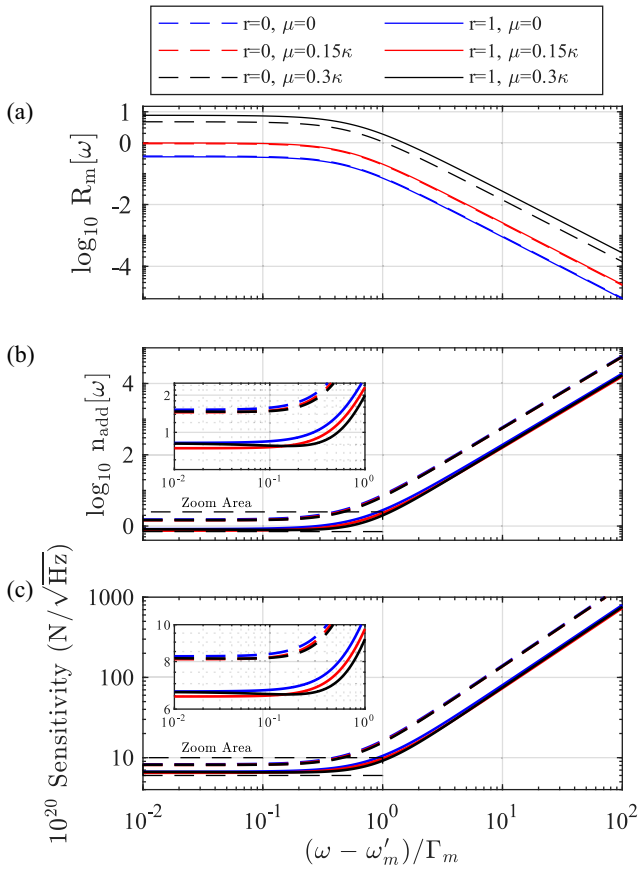


FIG. 4. (a) Off-resonant mechanical response $R_m[\omega]$, (b) optically added noise $n_{\text{add}}[\omega]$, and (c) force sensitivity as a function of the normalized frequency for different values of feedback gain and squeezing levels, with the other parameters fixed. Solid lines represent squeezed light ($\theta = 58.50^\circ$, $\theta_{\text{fb}} = 270^\circ$, and $\alpha = 60.84^\circ$) and dashed lines represent coherent light ($\theta = 45.40^\circ$ and $\theta_{\text{fb}} = 297.39^\circ$). Here $C = 0.1$ and $r = 1$. The other parameters are given in Table I.

Figure 3(a) illustrates the force sensitivity as a function of the measurement angle $\theta$ and the squeezed angle $\alpha$, with the other parameters are fixed. The region between the black (below) and white (above) dashed lines denotes the signal amplification $R_m[0] > 1$ and the added measurements noises suppression $n_{\text{add}}[0] < 0.8$ (0.8 is the minimum measurement noise achieved by coherent light without feedback). We see that amplitude quadrature squeezing (squeezed angle $\alpha = \pi/2$) and measurement angle $\theta = \pi/2$ (phase quadrature) are preferable to achieve the optimal sensitivity for on-resonance mechanical response in $C = 0.25$.

Figure 3(b) shows the force sensitivity as a function of the detuning $\Delta$ and feedback delay angle $\theta_{\text{fb}}$, with the other parameters kept fixed. A transparent light gray shaded area denotes the added measurement noise suppression and the signal amplification. We find that there exist multiple combinations of the detuning $\Delta$ and feedback delay angle $\theta_{\text{fb}}$ that can achieve the optimal sensitivity. Figure 3(b) indicates that the best force sensitivity can be achieved when the feedback delay angle $\theta_{\text{fb}}$ is around 0 and $1.5\pi$. Note that the feedback delay phase angle and the detuning and measurement angles

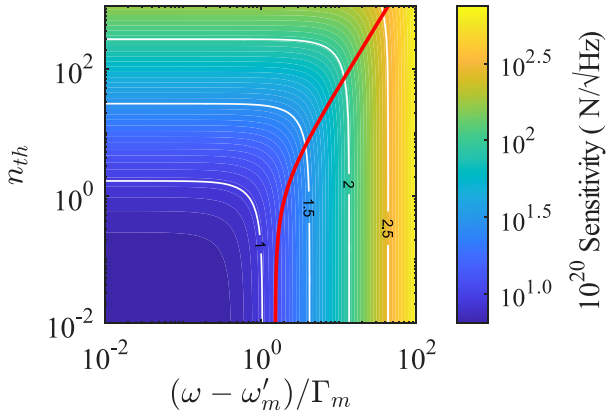


FIG. 5. Force sensitivity as a function of thermal phonon number and normalized frequency. The parameters are $\theta = 58.50^\circ$, $\alpha = 60.84^\circ$, $\theta_{\text{fb}} = 270^\circ$, $r = 1$, $\mu = 0.15\kappa$, $\Delta = \sqrt{\omega_m^2 + \kappa^2/4}$, and $C = 0.1$. White lines denote the contour line of the sensitivity and the red line denotes the sensitivity bandwidth (defined as a 3-dB degradation of the sensitivity) versus the thermal phonon number.

collectively form the global phase of the system's measurement. The optimal global phase is determined by various parameters of the system, such as the detection efficiency $\eta$, optomechanical cooperativity $C$, and feedback gain $g_{\text{fb}}$. Under the current set of parameters, the feedback delay phase at around 0 or $1.5\pi$ can increase the response of the mechanical oscillator $R_m[0]$ and reduce the measurement noise $n_{\text{add}}[0]$, thereby enhancing the measurement sensitivity.

### B. Off-resonance mechanical response and optically added noise

The off-resonant optically added noise, mechanical response, and the force sensitivity as a function of the normalized frequency for different feedback gain and squeezing levels are illustrated in Fig. 4. We see that increasing the feedback gain improves the amplification of the force signal while the bandwidth remains almost unchanged. Under fixed feedback gain, the squeezing has no effect on the signal amplification, as shown in Fig. 4(a). Figure 4(b) shows that the squeezing suppresses the optically added noise. When associated with appropriate feedback gain, the added noise reaches its minimum values. At a normalized frequency deviation of $\omega - \omega_m = 0.02 \times \Gamma_m$, the use of squeezed light without feedback leads to a 1.85-dB improvement in force sensitivity compared to the coherent light without feedback control, as shown by the blue dashed line in Fig. 4(c), highlighting the inherent benefit of squeezing. In contrast, the use of squeezed light with appropriate feedback enables a force sensitivity enhancement of 2.12 dB, as shown by the red solid line in Fig. 4(c).

### C. Sensitivity of the system with different initial phonon number

In the above analysis, we assume the initial phonon number to be $n_{\text{th}} = 0$. Figure 5 illustrates the force sensitivity as a function of the thermal phonon number and normalized frequency. Thermal noise is shown to greatly reduce the force sensitivity of the optomechanical system. Therefore, the cooling of the environment to ensure a low thermal noise number [20,30,32–37] is crucial to achieve a

high-precision force sensing. For example, a system operating at zero temperature ($n_{\rm th} = 0$) can realize a sensitivity of $S[\omega] = 6.5 \times 10^{-20}$ N/$\sqrt{\rm Hz}$. However, at room temperature ($T = 300$ K and $n_{\rm th} = 1.8 \times 10^7$), the sensitivity is degraded to $S[\omega] = 2.46 \times 10^{-16}$ N/$\sqrt{\rm Hz}$. Although the force sensitivity degrades with increasing initial phonon number, the sensitivity bandwidth (defined as a 3-dB degradation of the sensitivity) is broadened, as shown by the red line in Fig. 5. This can be explained using Eq. (34), from which the sensitivity bandwidth $\Delta\omega$ is determined by $n_{\rm add}[\Delta\omega] = 3(n_{\rm th} + \frac{1}{2} + 4/3 n_{\rm add}[0])$. This relation shows that $\Delta\omega$ scales linearly with $n_{\rm th}$.

## IV. EXPERIMENTAL FEASIBILITY

In this section we discuss the experimental feasibility of the proposed scheme. First, the parameters of the mechanical resonator, optical cavity, and effective detection efficiency, as list in Table I, are all achievable with the state-of-the-art technology. In Ref. [30], enhanced sideband cooling by feedback-controlled light was implemented in a resolved-sideband optomechanical system. To adapt to our scheme, it is straightforward to redesign the optomechanical system to operate in an unresolved sideband by shortening the Fabry-Perot cavity. Note that ground-state cooling via feedback techniques has been experimentally realized in an unresolved-sideband cavity optomechanical system [20].

To address the need for separate feedback systems of the mechanical resonator's cooling and weak-force sensing, we propose to employ two laser fields that are separated by one free spectral range of the optomechanical cavity. More precisely, coherent light with a wavelength of $\lambda_1$ is employed to implement the feedback cooling loop to prepare the membrane in the ground state. Subsequently, the squeezed light $\lambda_2$ with a readily available squeezing parameter of [38] is used for the weak-force measurement according to Fig. 1. In summary, the key components of our scheme, ground-state cooling and squeezed-light-enhanced weak-force measurement, are feasible with current technology.

## V. CONCLUSION

We have proposed a high-precision weak-force sensing scheme that utilizes squeezed light and feedback control in an unresolved-sideband cavity optomechanical system. By combining the injection of squeezed light with measurement-based feedback, such optomechanical systems can function as highly sensitive force sensors. The feedback-controlled in-loop light effectively amplifies the force signal, while the squeezed light significantly suppresses measurement noise. The combination of these two approaches improves the force sensitivity to approximately the order of $10^{-20}$ N/$\sqrt{\rm Hz}$ near the mechanical resonance frequency. This scheme is implemented in an unresolved-sideband cavity optomechanical configuration, which is technically easier and more feasible than systems operating in the resolved-sideband regime. In our scheme, the results of the force sensitivity are affected by the appropriate selection of various parameters. Machine learning may be used to quickly optimize the force sensitivity by searching the setting of multiple parameters. On the other hand, the current measurement system is based on analysis in the frequency domain. The measurement time equals the integration time of the spectral measurement, which is long enough to cover the dynamics of the system. We leave for future work the analysis of the weak-force measurement in the time domain and the dynamical capture of weak-force signals using a Lie-algebra decoupling framework [39]. In addition, our scheme may be applied to multimechanical mode optomechanical systems by tuning phonon-hopping interactions [40]. It is possible to enable enhanced control over the measurable bandwidth.

## ACKNOWLEDGMENTS

This work was supported by the National Natural Science Foundation of China (Grant No. 11774209) and Basic Research Program of Shanxi Province (Grant No. 202503021211060). The authors thank Dr. Bemani for the discussion on system stability.

## DATA AVAILABILITY

The data that support the findings of this article are not publicly available upon publication because it is not technically feasible and/or the cost of preparing, depositing, and hosting the data would be prohibitive within the terms of this research project. The data are available from the authors upon reasonable request.

## APPENDIX A: SCATTERING MATRIX ELEMENTS

The susceptibilities of the cavity field and the mechanical oscillator are given by

$$\chi_{\rm c}^{-1}[\omega] = -{\rm i}\Delta + {\rm i}\omega - \kappa_{\rm fb}/2, \tag{A1}$$

$$\chi_m^{-1}[\omega] = -{\rm i}\omega_m + {\rm i}\omega - \Gamma_m/2. \tag{A2}$$

Using $\chi_{\rm c}^*[\omega] = (\chi_{\rm c}[-\omega])^*$ and $\chi_{\rm m}^*[\omega] = (\chi_{\rm m}[-\omega])^*$, we obtain the matrix elements $s_{ij}$ $(i, j = 1, \ldots, 4)$ as

$$S_{11} = \sqrt{\kappa_1\kappa_{\rm fb}}\{4G^2\chi_{\rm c}^*[\omega](\chi_m[\omega] - \chi_m^*[\omega]) + \Gamma_m^2\chi_m[\omega]\chi_m^*[\omega] - 4\}Z, \tag{A3}$$

$$S_{12} = \sqrt{\kappa_1\kappa_{\rm fb}}\chi_{\rm c}[\omega]\chi_{\rm c}^*[\omega]\{4G^2(\chi_m[\omega] - \chi_m^*[\omega]) + \Lambda(4 - \Gamma_m^2\chi_m[\omega]\chi_m^*[\omega])\}Z, \tag{A4}$$

$$S_{13} = 2{\rm i}G\sqrt{\kappa_1\Gamma_m}\chi_{\rm c}[\omega]\chi_m[\omega](1 + \Lambda\chi_{\rm c}^*[\omega]) \times (\Gamma_m\chi_m^*[\omega] - 2)Z, \tag{A5}$$

$$S_{14} = 2{\rm i}G\sqrt{\kappa_{\rm s1}\Gamma_m}\chi_{\rm c}[\omega]\chi_m^*[\omega] \times (1 + \Lambda\chi_{\rm c}^*[\omega])(-2 + \Gamma_m\chi_m[\omega])Z, \tag{A6}$$

$$S_{21} = \sqrt{\kappa_{\rm s1}\kappa_{\rm fb}}\chi_{\rm c}[\omega]\chi_{\rm c}^*[\omega]\{4G^2(\chi_m^*[\omega] - \chi_m[\omega]) + \Lambda^*(4 - \Gamma_m^2\chi_m[\omega]\chi_m^*[\omega])\}Z, \tag{A7}$$

$$S_{22} = \sqrt{\kappa_{\rm s1}\kappa_{\rm fb}^*}\chi_{\rm c}^*[\omega]\{4G^2\chi_{\rm c}[\omega](\chi_m^*[\omega] - \chi_m[\omega]) + \Gamma_m^2\chi_m[\omega]\chi_m^*[\omega] - 4\}Z, \tag{A8}$$

$$S_{23} = -2{\rm i}G\sqrt{\kappa_{\rm s1}\Gamma_m}\chi_{\rm c}^*[\omega]\chi_m[\omega] \times (1 + \Lambda^*\chi_{\rm c}[\omega])(-2 + \Gamma_m\chi_m^*[\omega])Z, \tag{A9}$$

$$S_{24} = -2iG\sqrt{\kappa_{s1}\Gamma_m}\chi_c^*[\omega]\chi_m^*[\omega] \times (1+\Lambda^*\chi_c[\omega])(-2+\Gamma_m\chi_m[\omega])Z, \quad \text{(A10)}$$

$$S_{31} = 2iG\sqrt{\kappa_{fb}\Gamma_m}\chi_c[\omega]\chi_m[\omega] \times (\Lambda^*\chi_c^*[\omega]-1)(2+\Gamma_m\chi_m^*[\omega])Z, \quad \text{(A11)}$$

$$S_{32} = 2iG\sqrt{\kappa_{fb}^*\Gamma_m}\chi_c^*[\omega]\chi_m[\omega] \times (\Lambda\chi_c[\omega]-1)(2+\Gamma_m\chi_m^*[\omega])Z, \quad \text{(A12)}$$

$$S_{33} = 4\Gamma_m\chi_m[\omega](|\Lambda|^2\chi_c[\omega]\chi_c^*[\omega] + G^2\chi_m^*[\omega]\{\chi_c[\omega]-\chi_c^*[\omega] + (\Lambda-\Lambda^*)\chi_c[\omega]\chi_c^*[\omega]\}-1)Z, \quad \text{(A13)}$$

$$S_{34} = 2\Gamma_m\chi_m[\omega]\chi_m^*[\omega](2G^2\{\chi_c[\omega]-\chi_c^*[\omega] + (\Lambda-\Lambda^*)\chi_c[\omega]\chi_c^*[\omega]\} + \Gamma_m(1-|\Lambda|^2\chi_c[\omega]\chi_c^*[\omega]))Z, \quad \text{(A14)}$$

$$S_{41} = -2iG\sqrt{\kappa_{fb}\Gamma_m}\chi_c[\omega]\chi_m^*[\omega] \times (\Lambda^*\chi_c^*[\omega]-1)(2+\Gamma_m\chi_m[\omega])Z, \quad \text{(A15)}$$

$$S_{42} = -2iG\sqrt{\kappa_{fb}^*\Gamma_m}\chi_c^*[\omega]\chi_m^*[\omega] \times (\Lambda\chi_c[\omega]-1)(2+\Gamma_m\chi_m[\omega])Z, \quad \text{(A16)}$$

$$S_{43} = -2\Gamma_m\chi_m[\omega]\chi_m^*[\omega](2G^2\{\chi_c[\omega]-\chi_c^*[\omega] + (\Lambda-\Lambda^*)\chi_c[\omega]\chi_c^*[\omega]\} + \Gamma_m(-1+|\Lambda|^2\chi_c[\omega]\chi_c^*[\omega]))Z, \quad \text{(A17)}$$

$$S_{44} = 4\Gamma_m\chi_m^*[\omega](|\Lambda|^2\chi_c[\omega]\chi_c^*[\omega] + G^2\chi_m[\omega]\{\chi_c^*[\omega]-\chi_c[\omega] + (\Lambda^*-\Lambda)\chi_c[\omega]\chi_c^*[\omega]\}-1)Z. \quad \text{(A18)}$$

Here $Z$ is defined as

$$Z = (4G^2\{\chi_c^*[\omega]-\chi_c[\omega]+(\Lambda^*-\Lambda)\chi_c[\omega] \times \chi_c^*[\omega]\}(\chi_m[\omega]-\chi_m^*[\omega]) + \Gamma_m^2\chi_m[\omega]\chi_m^*[\omega]+4|\Lambda|^2\chi_c[\omega]\chi_c^*[\omega] - |\Lambda|^2\chi_c[\omega]\chi_c^*[\omega]\Gamma_m^2\chi_m[\omega]\chi_m^*[\omega]-4)^{-1}. \quad \text{(A19)}$$

## APPENDIX B: SYSTEM STABILITY

When all eigenvalues of the drift matrix $A$ have negative real parts, the system is stable [41]. However, directly solving for the roots of higher-order characteristic equations is often analytically intractable, particularly in complex systems. This has led to the demand for algebraic methods that can determine stability without explicitly solving the equations. The Routh-Hurwitz criterion is a classical method for assessing the stability of feedback control systems. It constructs the Routh array based solely on the coefficients of the characteristic equation polynomials. When the signs of the elements in the first column are consistent, the stability of the system can be efficiently determined. The algebraic nature of this method renders it particularly advantageous for engineering practice. The elements of the first column ($C_1$, $C_2$, $C_3$, and $C_4$) in the Routh array are given by

$$C_1 = \Gamma_m + K_1 > 0, \quad \text{(B1)}$$

$$C_2 = 2K_1(4\Gamma_m^2+4\Gamma_mK_1+K_2)+8\Gamma_m\omega_m^2 > 0, \quad \text{(B2)}$$

$$C_3 = -4G^2K_3\omega_m + \frac{K_2}{4}\omega_m^2 > 0, \quad \text{(B3)}$$

$$C_4 = \frac{K_2}{4}\Gamma_mC_2 + K_1C_2\omega_m^2 - C_1C_3 > 0, \quad \text{(B4)}$$

where $K_1 = \kappa + 2\mu\cos(\theta_{fb}-\theta)$, $K_2 = 4\Delta^2+\kappa^2+8\Delta\mu\sin(\theta_{fb}-\theta)+4\mu\kappa\cos(\theta_{fb}-\theta)$, and $K_3 = \Delta+\mu\sin(\theta_{fb}-\theta)-\mu\sin(\theta_{fb}+\theta)$.

## APPENDIX C: DYNAMIC BACKACTION

In this appendix we discuss how optical backaction influences the mechanical system. In the case of nonzero feedback gain ($g_{fb} \neq 0$) and nonzero detuning ($\Delta \neq 0$), the dynamics of the system become increasingly complex because of the mutual coupling between the amplitude and the phase of the optical field, both of which are additionally coupled to the mechanical system. Equation (32) can be rewritten as

$$\eta R_m[\omega] = 2\Gamma_m f_{imp}|\chi_{eff}[\omega]|^2, \quad \text{(C1)}$$

where

$$f_{imp} = G^2\eta\kappa_{s1}(|\chi_c[\omega]|^2\{1+2\,\mathrm{Re}(\Lambda^*\chi_c[-\omega]) + |\Lambda|^2|\chi_c[-\omega]|^2\}+|\chi_c[-\omega]|^2\{1+2\,\mathrm{Re}(\Lambda^*\chi_c[\omega]) + |\Lambda|^2|\chi_c[\omega]|^2\}-2\,\mathrm{Re}\{e^{2i\theta}\chi_c^*[-\omega]\chi_c^*[\omega] \times (1+\Lambda^*\chi_c[-\omega])(1+\Lambda^*\chi_c[\omega])\}), \quad \text{(C2)}$$

$$|\chi_{eff}[\omega]| = 2|i(|\chi_m[\omega]-\chi_m^*[\omega]|)Z[\omega]|, \quad \text{(C3)}$$

and $\chi_m[\omega]$, $\chi_c[\omega]$, and $Z[\omega]$ are given in Appendix A. Here $f_{imp}$ is the transfer function between the displacement spectrum and the optical quadrature spectrum and $|\chi_{eff}[\omega]|^2$ defines the modified mechanical susceptibility, which is expressed as the original mechanical susceptibility $\chi_Q$ and an additional term $\Xi$. This modification has the form of a "self-energy" [26]

$$\chi_{eff}[\omega]^{-1} = \chi_Q[\omega]^{-1}+\Xi[\omega] = \frac{{\omega_m}^2+2\omega\omega_{opt}-\omega^2-i\omega(\Gamma_m+\Gamma_{opt})}{\omega_m}. \quad \text{(C4)}$$

From Eq. (C4) we can obtain the frequency-dependent optomechanical damping rate $\Gamma_{opt}[\omega] = -\omega_m\,\mathrm{Im}(\Xi[\omega])/\omega$ and mechanical frequency shift $\omega_{opt} = \omega_m\,\mathrm{Re}(\Xi[\omega])/2\omega$. We then define a modified frequency-dependent mechanical resonant frequency $\omega_m' \equiv \omega_m+\omega_{opt}$ and an effective damping $\Gamma_m' \equiv \Gamma_m+\Gamma_{opt}$.

An analytical solution for $\Xi[\omega]$, which determines the optomechanical damping rate $\Gamma_{opt}[\omega] = -\omega_m\,\mathrm{Im}(\Xi[\omega])/\omega$ and the mechanical frequency shift $\omega_{opt} = \omega_m\,\mathrm{Re}(\Xi[\omega])/2\omega$, is

$$\Xi[\omega] = 2G^2(i\chi_c[\omega]-i\chi_c^*[\omega]) + \frac{1}{\omega_m}\big[\mu^2(\omega^2-\omega_m^2+i\Gamma_m\omega) + 2\mu G^2\omega_m\sin(\theta_{fb}+\theta)\big]\chi_c[\omega]\chi_c^*[\omega]. \quad \text{(C5)}$$

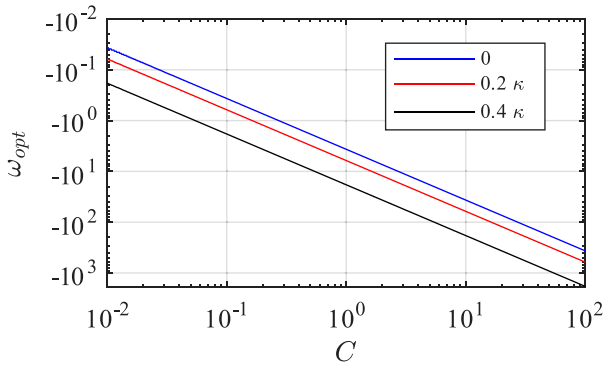


FIG. 6. Plot of the characteristic frequency shift of the mechanical oscillator due to the optical spring effect varying with $C$. The same plotting parameters as in Fig. 2 were used.

Its real and imaginary parts are

$$\mathrm{Re}(\Xi[\omega]) = \frac{N_R}{D_R}, \tag{C6}$$

where

$$\begin{aligned} N_R =& 4\{[-4\Delta G^2\omega_m + \mu^2(\omega^2-\omega_m^2) \\ &+ 2G^2\mu\omega_m\sin(\theta_{\rm fb}+\theta) \\ &- 4G^2\mu\omega_m\sin(\theta_{\rm fb}-\theta)][4\Delta^2+4\mu^2+\kappa^2-4\omega^2 \\ &+ 4\kappa\mu\cos(\theta_{\rm fb}-\theta)+8\Delta\mu\sin(\theta_{\rm fb}-\theta)] \\ &- 4\Gamma_m\mu^2\omega^2[\kappa+2\mu\cos(\theta_{\rm fb}-\theta)]\}, \end{aligned} \tag{C7}$$

$$\begin{aligned} D_R =& \omega_m\{[4\Delta^2+4\mu^2+\kappa^2-4\omega^2+4\kappa\mu\cos(\theta_{\rm fb}-\theta) \\ &+ 8\Delta\mu\sin(\theta_{\rm fb}-\theta)]^2+16\omega^2[\kappa+2\mu\cos(\theta_{\rm fb}-\theta)]^2\}, \end{aligned} \tag{C8}$$

and

$$\mathrm{Im}(\Xi[\omega]) = \frac{N_I}{D_I}, \tag{C9}$$

where

$$\begin{aligned} N_I =& 4\{\Gamma_m\mu^2\omega[4\Delta^2+4\mu^2+\kappa^2-4\omega^2 \\ &+ 4\kappa\mu\cos(\theta_{\rm fb}-\theta)+8\Delta\mu\sin(\theta_{\rm fb}-\theta)] \\ &+ 4\omega[\kappa+2\mu\cos(\theta_{\rm fb}-\theta)][-4\Delta G^2\omega_m \\ &+ \mu^2(\omega^2-\omega_m^2)+2G^2\mu\omega_m\sin(\theta_{\rm fb}+\theta) \\ &- 4G^2\mu\omega_m\sin(\theta_{\rm fb}-\theta)]\}, \end{aligned} \tag{C10}$$

$$D_I = D_R. \tag{C11}$$

When $\mu = 0$ and $\omega = \omega_m$, Eqs. (C6) and (C9) are consistent with previous results using a sufficiently weak laser, as shown in [24]. As indicated by Eq. (C6), the mechanical frequency shift is determined by the detuning $\Delta$, the feedback gain $\mu$, the phase angle of the feedback delay $\theta_{\rm fb}$, and the measurement angle $\theta$ under $C$ and $r$. Figure 6 shows the frequency shift of the mechanical resonator versus $C$, with other parameters held constant. The resonance frequency in Fig. 2 refers to the characteristic frequency of the mechanical resonator incorporating the frequency shift shown in Fig. 6.

## APPENDIX D: ADDED NOISE OF MEASUREMENT

The added noise of measurement $n_{\rm add}[\omega]$ characterizes the effective increase of the thermal excitations of the mechanical reservoir arising from the backaction of the optical mode. It consists of the backaction noise, imprecision noise, and the quantum correlations between the imprecision and backaction and is given by

$$\begin{aligned} n_{\rm add}[\omega] =& \frac{1}{R_m[\omega]}\Bigg[\frac{1}{2}(\Psi[\omega]\Psi^*[-\omega]+\Psi[-\omega]\Psi^*[\omega])\frac{1}{|\kappa_{\rm fb}|}\Bigg[\frac{K_1}{2}+\frac{\mu^2}{\kappa_{\rm s1}\eta}+\left(K_1+\frac{2\mu^2}{\kappa_{\rm s1}}\right)\zeta\sinh^2(r) \\ &+\left(\mu\cos(\theta_{\rm fb}+\theta-2\alpha)+\frac{\mu^2}{\kappa_{\rm s1}}\cos(2\theta-2\alpha)\right)\zeta\sinh(2r)\Bigg]+\mathrm{Re}\Bigg(\Psi^*[\omega]\Psi^*[-\omega]\frac{1}{\kappa_{\rm fb}^*}\Bigg\{K_6+\frac{4K_5^2}{\eta} \\ &+(2K_6+8K_5^2)\zeta\sinh^2(r)+\left[\left(\sqrt{\kappa_{\rm s1}}K_4-\frac{\kappa_{\rm s1}}{2}\right)e^{-2i\alpha}+4K_5^2\cos[2(\alpha-\theta)]\right]\zeta\sinh(2r)\Bigg\}\Bigg) \\ &+\mathrm{Re}\Bigg[e^{-i\theta}(\Psi^*[-\omega]+\Psi^*[\omega])\frac{1}{\sqrt{\kappa_{\rm fb}^*}}\left(\frac{K_4}{2}+K_4\zeta\sinh^2(r)+K_5e^{-i\theta}e^{2i\alpha}\zeta\sinh(2r)\right)\Bigg] \\ &+\mathrm{Re}\Bigg\{e^{i\theta}(\Psi^*[-\omega]+\Psi^*[\omega])\frac{1}{\sqrt{\kappa_{\rm fb}^*}}\left[K_5e^{-i\theta}+2K_5e^{-i\theta}\zeta\sinh^2(r)+\left(\frac{\sqrt{\kappa_{\rm s1}}}{2}+K_5e^{i\theta}\right)e^{-2i\alpha}\zeta\sinh(2r)\right]\Bigg\} \\ &+\frac{1}{2}+\zeta\sinh^2(r)+\frac{\cos[2(\alpha-\theta)]}{2}\zeta\sinh(2r)+\frac{1-\eta}{2\eta}\Bigg], \end{aligned} \tag{D1}$$

where

$$K_1 = \kappa + 2\mu\cos(\theta_{\rm fb}-\theta), \tag{D2}$$

$$K_4 = \sqrt{\kappa_{\rm s1}} + \frac{\mu}{\sqrt{\kappa_{\rm s1}}}e^{-i(\theta_{\rm fb}-\theta)}, \tag{D3}$$

$$K_5 = \frac{\mu}{2\sqrt{\kappa_{\rm s1}}}e^{-i\theta_{\rm fb}}, \tag{D4}$$

$$K_6 = \mu e^{-i(\theta_{\rm fb}+\theta)}. \tag{D5}$$

[1] A. N. Jordan and I. A. Siddiqi, *Quantum Measurement: Theory and Practice*, 1st ed. (Cambridge University Press, Cambridge, 2024).

[2] C. L. Degen, F. Reinhard, and P. Cappellaro, Quantum sensing, Rev. Mod. Phys. **89**, 035002 (2017).

[3] B. P. Abbott *et al.* (LIGO Scientific Collaboration and Virgo Collaboration), Observation of gravitational waves from a binary black hole merger, Phys. Rev. Lett. **116**, 061102 (2016).

[4] J. Abadie *et al.* (LIGO Scientific Collaboration), A gravitational wave observatory operating beyond the quantum shot-noise limit, Nat. Phys. **7**, 962 (2011).

[5] U. Mohideen and A. Roy, Precision measurement of the Casimir force from 0.1 to 0.9 μm, Phys. Rev. Lett. **81**, 4549 (1998).

[6] C. Clavaud, M. Maza-Cuello, C. Frétigny, L. Talini, and T. Bickel, Modification of the fluctuation dynamics of ultrathin wetting films, Phys. Rev. Lett. **126**, 228004 (2021).

[7] T. Gisler, D. Hälg, V. Dumont, S. Misra, L. Catalini, E. C. Langman, A. Schliesser, C. L. Degen, and A. Eichler, Enhancing membrane-based scanning force microscopy through an optical cavity, Phys. Rev. Appl. **22**, 044001 (2024).

[8] D. Rugar, B. Stipe, H. Mamin, C. Yannoni, T. Stowe, K. Yasumura, and T. Kenny, Adventures in attonewton force detection, Appl. Phys. A **72**, S3 (2001).

[9] X. Shan, L. Ding, D. Wang, S. Wen, J. Shi, C. Chen, Y. Wang, H. Zhu, Z. Huang, S. S. J. Wang, X. Zhong, B. Liu, P. J. Reece, W. Ren, W. Hao, X. Lu, J. Lu, Q. P. Su, L. Chang, L. Sun, *et al.*, Sub-femtonewton force sensing in solution by super-resolved photonic force microscopy, Nat. Photonics **18**, 913 (2024).

[10] J. Aasi *et al.* (LIGO Scientific Collaboration and Virgo Collaboration), Enhanced sensitivity of the LIGO gravitational wave detector by using squeezed states of light, Nat. Photonics **7**, 613 (2013).

[11] M. A. Taylor, J. Janousek, V. Daria, J. Knittel, B. Hage, H.-A. Bachor, and W. P. Bowen, Biological measurement beyond the quantum limit, Nat. Photonics **7**, 229 (2013).

[12] D. D. Wang, Q. S. Wang, Q. Zhang, and Y. M. Li, Ultrasensitive displacement measurement with nonlinear optomechanical coupling and squeezed light injection, J. Opt. Soc. Am. B **40**, 604 (2023).

[13] Q. Li, W. Li, Y. Wang, Y. Wang, L. Tian, S. Shi, and Y. Zheng, Quantum-enhanced optomechanical sensor network, Laser Photonics Rev. **20**, e01636 (2025).

[14] H. Yu, L. McCuller, *et al.* (LIGO Scientific Collaboration), Quantum correlations between light and the kilogram-mass mirrors of LIGO, Nature (London) **583**, 43 (2020).

[15] S.-D. Zhang, J. Wang, Q. Zhang, Y.-F. Jiao, Y.-L. Zuo, Ş. K. Özdemir, C.-W. Qiu, F. Nori, and H. Jing, Squeezing-enhanced quantum sensing with quadratic optomechanics, Opt. Quantum **2**, 222 (2024).

[16] S. Zhang, J. Wang, Q. Zhang, H. Lin, and H. Jing, Quantum squeezing-enhanced supersensitive optomechanical sensing, Laser Optoelectron. Prog. **62**, 1127004 (2025).

[17] S.-L. Chao, Z.-H. Li, and X.-Y. Lü, Enhancing force sensing in a squeezed optomechanical system with quantum non-demolition measurement, Commun. Theor. Phys. **76**, 015104 (2024).

[18] W. Qin, A. Miranowicz, and F. Nori, Exponentially improved dispersive qubit readout with squeezed light, Phys. Rev. Lett. **133**, 233605 (2024).

[19] D. Xie and C. Xu, Dispersive qubit readout of temperature, Phys. Rev. A **111**, 062412 (2025).

[20] M. Rossi, D. Mason, J. Chen, Y. Tsaturyan, and A. Schliesser, Measurement-based quantum control of mechanical motion, Nature (London) **563**, 53 (2018).

[21] F. Bemani, O. Černotík, L. Ruppert, D. Vitali, and R. Filip, Force sensing in an optomechanical system with feedback-controlled in-loop light, Phys. Rev. Appl. **17**, 034020 (2022).

[22] J. Bennett, Quantum optomechanics in the unresolved sideband regime, Ph.D. thesis, University of Queensland, 2017.

[23] S. Zippilli, N. Kralj, M. Rossi, G. Di Giuseppe, and D. Vitali, Cavity optomechanics with feedback-controlled in-loop light, Phys. Rev. A **98**, 023828 (2018).

[24] W. P. Bowen and G. J. Milburn, *Quantum Optomechanics*, 1st ed. (CRC, Boca Raton, 2015).

[25] M. Asjad, S. Zippilli, and D. Vitali, Suppression of stokes scattering and improved optomechanical cooling with squeezed light, Phys. Rev. A **94**, 051801(R) (2016).

[26] *Cavity Optomechanics: Nano- and Micromechanical Resonators Interacting with Light*, edited by M. Aspelmeyer, T. J. Kippenberg, and F. Marquardt (Springer, Berlin, 2014).

[27] S. S. Zheng, F. X. Sun, M. Asjad, G. W. Zhang, J. Huo, J. Li, J. Zhou, Z. Ma, and Q. Y. He, Optomechanical cooling with simultaneous intracavity and extracavity squeezed light, Phys. Rev. A **110**, 063520 (2024).

[28] J.-H. Gan, Y.-C. Liu, C. Lu, X. Wang, M. K. Tey, and L. You, Intracavity-squeezed optomechanical cooling, Laser Photonics Rev. **13**, 1900120 (2019).

[29] X. Xu and J. M. Taylor, Squeezing in a coupled two-mode optomechanical system for force sensing below the standard quantum limit, Phys. Rev. A **90**, 043848 (2014).

[30] M. Rossi, N. Kralj, S. Zippilli, R. Natali, A. Borrielli, G. Pandraud, E. Serra, G. Di Giuseppe, and D. Vitali, Enhancing sideband cooling by feedback-controlled light, Phys. Rev. Lett. **119**, 123603 (2017).

[31] *Quantum Optomechanics and Nanomechanics*, edited by P.-F. Cohadon, J. Harris, F. Marquardt, and L. Cugliandolo, Proceedings of the Les Houches Summer School of Theoretical Physics, CV, 2015 (Oxford University Press, Oxford, 2020), pp. 1–40.

[32] D. J. Wilson, V. Sudhir, N. Piro, R. Schilling, A. Ghadimi, and T. J. Kippenberg, Measurement-based control of a mechanical oscillator at its thermal decoherence rate, Nature (London) **524**, 325 (2015).

[33] J. Chan, T. P. M. Alegre, A. H. Safavi-Naeini, J. T. Hill, A. Krause, S. Gröblacher, M. Aspelmeyer, and O. Painter, Laser cooling of a nanomechanical oscillator into its quantum ground state, Nature (London) **478**, 89 (2011).

[34] J. D. Teufel, T. Donner, D. Li, J. W. Harlow, M. S. Allman, K. Cicak, A. J. Sirois, J. D. Whittaker, K. W. Lehnert, and R. W. Simmonds, Sideband cooling of micromechanical motion to the quantum ground state, Nature (London) **475**, 359 (2011).

[35] F. Tebbenjohanns, M. L. Mattana, M. Rossi, M. Frimmer, and L. Novotny, Quantum control of a nanoparticle optically levitated in cryogenic free space, Nature (London) **595**, 378 (2021).

[36] U. Delić, M. Reisenbauer, K. Dare, D. Grass, V. Vuletić, N. Kiesel, and M. Aspelmeyer, Cooling of a levitated nanoparticle

to the motional quantum ground state, Science **367**, 892 (2020).

[37] J. B. Clark, F. Lecocq, R. W. Simmonds, J. Aumentado, and J. D. Teufel, Sideband cooling beyond the quantum backaction limit with squeezed light, Nature (London) **541**, 191 (2017).

[38] H. Vahlbruch, M. Mehmet, K. Danzmann, and R. Schnabel, Detection of 15 dB squeezed states of light and their application for the absolute calibration of photoelectric quantum efficiency, Phys. Rev. Lett. **117**, 110801 (2016).

[39] S. Qvarfort and I. Pikovski, Solving quantum dynamics with a Lie-algebra decoupling method, PRX Quantum **6**, 010201 (2025).

[40] D.-h. Xu, Z. Liu, and C.-s. Yu, Enhancing optomechanical force sensing utilizing synthetic magnetism, Phys. Rev. A **111**, 053508 (2025).

[41] E. X. DeJesus and C. Kaufman, Routh-Hurwitz criterion in the examination of eigenvalues of a system of nonlinear ordinary differential equations, Phys. Rev. A **35**, 5288 (1987).